2022 IEEE/RSJ International Conference on Intelligent Robots and Systems (IROS 2022)
October 23-27, 2022, Kyoto, Japan

Improved biped walking performance around the kinematic singularities of biomimetic four-bar knees

Aikaterini Smyrli,* *Student Member, IEEE*, and Evangelos Papadopoulos, *Fellow, IEEE*

***Abstract*— This paper studies the effects of replacing pin-joint knees in passive dynamic bipedal walkers with biomimetic four-bar knees. The kinetic model of the four-bar knees is presented in detail, and an analytical model of the passive walking dynamics is derived. The resulting four-bar kneed biped is compared with a pin-joint kneed walker, for their passive walking performance. The geometry of the four-bar knees used in the study is based on human anatomical data. It is found that the biomimetic four-bar knee configuration works to the advantage of the biped, especially around the extended-knee singular position. The four-bar knees are found to overperform the pin-joint ones, resulting in significant reduction of peak impact loads and energetic expenditure.**

I. Introduction

The study of the gait dynamics of biped robots has been a key point of interest of the robotics community in the last decades. An attractive aspect of bipedal walking is its potential passivity: Mc Geer first demonstrated the ability of human-like biped robots to perform stable passive walking without any energetic or even corrective input [1]. This characteristic can -and has been- taken into advantage in designing energy-efficient, biomimetic walking robots and human leg prostheses.

The modeling of human gait can range from simple biped designs that move in an almost intuitive manner and offer useful insight into the basic gait dynamics [2], to complex multi-DoF humanoids, that are successful at performing complex functions of the human locomotion system [3].

Energetic efficiency has been demonstrated and studied for simple walkers [1][2], and it is a major consideration in designing complex walking robots, as smaller power expenditures translate to increasingly autonomous systems. Consequently, considerable effort has been focused on studying the passive dynamics of biped robots, that over the years are becoming increasingly similar to humans [4][5][6][7][8][9].

A key element of bipedal walking is the function of the knee: its flexion during the swing phase allows the advancement of the swing foot forward, avoiding contacts with the floor or with any other obstacles, while at its extension during the stance phase, it effectively supports the weight of the biped, preventing a collapse [1][8][9]. Due to its importance in achieving successful gait, knee design for biped robots presents an increased scientific interest. Studies have approached the knee design using pin joints [1][8][10], circular rolling elements [11][12], as well as open [13][14][15] and crossed [16][17] four-bar linkages.

The selection of the four-bar linkage as a knee mechanism is inspired by the human knee design, where the cruciate ligaments of the knee form a crossed four-bar linkage: a closed kinematic chain with the femoral and tibial bones, constraining their relative motion during knee flexion and extension [18][19]. Several studies on the knee's biomechanics have suggested the four-bar linkage as a suitable model to approximate the human knee [20], and various over-the-knee prostheses are designed based on this mechanism [21][22].

In this study, the passive dynamics of a biped walker with biomimetic four-bar knees are studied for the first time. The results are compared to the gait of a passive biped with pin joint knees, presented in [8]. The four-bar mechanism used in the model approximates the human knee, using human data sourced from biomechanical studies [19]. The study showcases significant results on impact force reduction, as well as increased energetic efficiency, both of which emerge from the increased passive compliance introduced when substituting the pin joint knees with four-bar linkages.

The four-bar kneed biped model is introduced and analyzed in Section II. Section III presents gait comparisons between the passive dynamic simulations of the two biped models, and Section IV discusses the significant effect of the four-bar knees in increasing energetic efficiency. Section V concludes the study.

II. Model of the Four-Bar Kneed Walker

A. Model Description

The biped model studied in this paper is an evolution of the passive kneed biped walker that has been developed and studied by our team in [8], shown in Fig. 1(a). In this study, the simple pin-joint knees of [8] and Fig. 1(a) are replaced by a bio-inspired four-bar kinematic linkage, presented in Fig. 1(b), to study the differences between the two designs.

Apart from their knee joints, the two models of Fig. 1 are identical in their design. Specifically, Fig. 1(a) shows the design parameters of the *joint knee* model (JK). The biped consists of two legs, joined together at the hip. The main inertial element of the biped is located at the hip joint, and is composed of a body of mass M and moment of inertia I. Each of the biped's legs is divided in the femoral and the tibial link, joined together at the knee. The femoral link of the biped has a point mass m_f, positioned across the femoral link and at a distance l_f from the knee joint. The femoral link's moment of inertia is I_f, and its total length is

*Corresponding author.
The authors are with the School of Mechanical Engineering, National Technical University of Athens, (e-mail: katerinasmyrli@mail.ntua.gr, egpapado@central.ntua.gr, tel: +30 210-772-1440).

The presentation of this paper was partially made possible through a travel grant by the "C. Mavroidis Award of Excellence in Robotics and Automation" at the NTUA.

L_f. The corresponding parameters of the tibial link are m_t, l_{ty}, I_t and L_t. The point mass of the tibial link is allowed an offset from the tibial link's axis, l_{tx}, which enables the accurate representation of the foot's inertial contribution.

The JK biped's knees are prevented from hyperextension by a viscoelastic kneecap, which impacts the knees at their fully extended position, when the femoral and tibial links are parallel. The linear viscoelastic kneecap is modelled as a spring k connected in parallel with a damper c [8].

The biped's biomimetic feet are defined according to the methodology introduced in [7]. Specifically, any convex geometry can be used as a footshape for the biped, the kinematics of which are numerically integrated into the biped's dynamics [7]. To note this, a set of points forming a convex curve are drawn as the footshape of the biped in Fig. 1(a) and Fig. 1(b).

Fig. 1(b) presents the *four bar* model (4B) of the passive biped, which differs from the JK model only in respect to the knee joints. Most of the JK biped's parameters, shown in Fig. 1(a), are defined identically in the 4B biped of Fig. 1(b) and are not repeated in the figure. The viscolelastic kneecap used in the two models is mechanically the same, but in the 4B biped it is positioned between two links of the four bar linkage, see Fig. 2.

The mechanical design of the knee affects the relative motion between the tibial and femoral links of the biped. More specifically, the *instantaneous center of rotation* (ICR) of the motion between the femoral and tibial links changes in the 4B biped: this is a kinematic characteristic of the four-bar linkage that connects them. In a crossed four-bar linkage, as is the case in this study, the position of the ICR coincides with the intersection of the two crossing links [19]. On the other hand, the position of the ICR in a pin joint is stationary at the joint position. To ensure that the JK and 4B models are as similar as possible apart from their knee design, some non-knee design parameters of the JK model must be re-defined in the 4B biped: the lengths L_f, L_t and l_{ty} in the 4B biped are defined from the position of the ICR in full knee extension, when the tibial and femoral links are parallel. Thus, the inertial properties of the two models are equivalent at full knee extension, but diverge slightly as the knees bend.

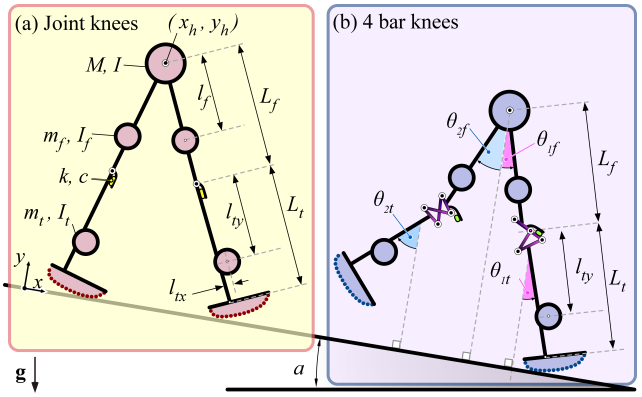

Fig. 1. Two biped models are compared. (a) Model of a passive biped robot with simple pin-joint knees, developed in [8]. (b) Model of the passive biped walker with biomimetic four-bar knees, introduced in this study.

The *generalized coordinates* (GCs) of both models are defined next. The first two GCs are the hip position on the (x, y) plane, defined by x_h and y_h. Next are the femoral link angles θ_{if}, where $i = 1, 2$ for Leg-1 and Leg-2 respectively. Finally, the angles at which the viscoelastic kneecaps act, θ_{ik}, are different for the two models, since their knee design is different. The GCs comprise the GC vector $\mathbf{q}$ which is 6x1 for both models:

$$\mathbf{q} = [x_h, y_h, \theta_{1f}, \theta_{1k}, \theta_{2f}, \theta_{2k},]^{\mathrm{T}} \tag{1}$$

The kneecap angles are defined using the tibial angles θ_{it}, but the definition is different for the JK and 4B models.

In the case of the JK biped, the definition is straightforward: the kneecap acts on the angle between the femoral and tibial links, and therefore the kneecap angle for the JK is:

$$^{\mathrm{JK}}\theta_{ik} = \theta_{if} - \theta_{it} \tag{2}$$

The relationship between the kneecap angle θ_{ik} and the tibial angle θ_{it} for the 4B biped is presented next.

B. Kinematic analysis of the four bar knee

Fig. 2(a) presents the general configuration of the 4B biped's knee. The four-bar mechanism is composed by four kinematic links, b_j for $j = 1, ..., 4$, which are joined by pin joints at points P_j. Table I presents the link definitions with respect to points P_j of Fig. 2. The four-bar linkage is fixed to the femoral link at point P_f of link b_3, forming an angle θ_{bf} with the femur. In a similar manner, the mechanism is fixed to the tibial link at point P_t of link b_1, forming an angle θ_{bt} with the tibia.

As is shown in Fig. 2(b), the kneecap of the 4B model acts on the internal angle ϕ of the four bar linkage, once this reduces below the limit value $\phi = 0$, depicted in Fig. 2(b). Therefore, we can write:

$$^{\mathrm{4B}}\theta_{ik} = \phi_i \tag{3}$$

Since ϕ is equal to one of the model's GCs, we assume its value is known, and aim to calculate the tibial angle θ_t (in this section, the index i will be emitted for simplicity).

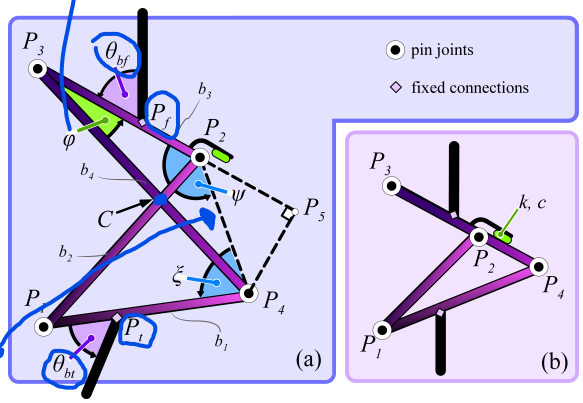

Fig. 2. Knee mechanism of the 4B biped model. (a) General configuration, for kneecap angle $\phi > 0$. The kneecap is inactive. (b) Knee strike at singular configuration. When $\phi = 0$ the viscoelastic kneecap first acts on ϕ.

First, the distance (P_2P_4) is calculated using the law of cosines for $(P_2\overset{\triangle}{P_3}P_4)$:

$$(P_2P_4) = \sqrt{b_3^2 + b_4^2 - 2b_3b_4cos(\phi)} \tag{4}$$

Then the sine of angle ψ is calculated using the law of sines for $(P_2\overset{\triangle}{P_3}P_4)$ in (5), and the cosine of ψ is found using the orthogonal triangle $(P_2\overset{\triangle}{P_5}P_4)$ in (6). From these we can find ψ in (7)

$$\sin(\psi) = \frac{b_4 \sin(\phi)}{(P_2P_4)} \tag{5}$$

$$\cos(\psi) = -\cos(\pi - \psi) = -\frac{l_4\cos(\phi) - b_3}{(P_2P_4)} \tag{6}$$

$$\psi(\phi) = \text{atan2}(b_4 sin(\phi), b_3 - b_4\cos(\phi)) \tag{7}$$

We can then find ξ from the law of cosines on $(P_1\overset{\triangle}{P_4}P_2)$. During the normal motion of the knee in humans $0 \leq \xi \leq \pi$, see Fig. 3, and therefore we ignore the negative solution of the inverse cosine function:

$$\xi(\phi) = \text{acos}\Big(\frac{b_1^2 + (P_2P_4)^2 - b_2^2}{2b_1(P_2P_4)}\Big) \tag{8}$$

Finally, we find θ_t as a function of θ_f and ${}^{4B}\theta_k = \phi$:

$$\theta_t = \theta_f + \theta_{bf} + \psi({}^{4B}\theta_k) + \xi({}^{4B}\theta_k) + \theta_{bt} \tag{9}$$

Using (7) and (8) we can calculate the positions of the points P_j, $j = 1..4$ on the (x, y) plane as a function of the GCs of the 4B biped model, and therefore the configuration of the four-bar knees as a function of $\mathbf{q}$. Similarly, we can find the ICR position, marked as point C in Fig. 2(a), which lies at the intersection of the crossing links of the 4B knee at each configuration.

Table I presents the 4B knee parameter values that are used in this study. The values of the parameters are based on human data [18]. The scaling parameter $L = 0.6$ scales the human parameters so that the 4B knees are dimensionally appropriate for the smaller-than-human scaled biped model.

TABLE I: PARAMETERS OF THE 4B KNEE.

Parameter name	Points in Fig. 2	Value
b_1	P_1P_4	$0.0305L$ [m]
b_2	P_1P_2	$0.0322L$ [m]
b_3	P_2P_3	$0.0128L$ [m]
b_4	P_3P_4	$0.0299L$ [m]
l_{1t}	P_1P_t	$b_1/2$ [m]
l_{3f}	P_3P_f	$b_3/2$ [m]
θ_{bf}	P_f	25.00 °
θ_{bt}	P_t	75.26 °

Fig. 3(a-d) shows the 4B knees for the parameter set of Table I, for various values of the kneecap angle ${}^{4B}\theta_k = \phi$. In the case of Fig. 3(a), ${}^{4B}\theta_k = \phi = 0$, the femoral and tibial links are parallel and the 4B knees are fully extended and in a *singular* configuration.

C. Around the kinematic singularity of the 4B knees

As mentioned in the previous section, the kneecap acts to constrain the kneecap angle when $\phi = {}^{4B}\theta_k \leq 0$, effectively stopping the knees from hyperextending. During the passive gait, the stance leg of the biped remains at this extended position, pressing against the activated kneecap and preventing a collapse of the biped for exactly half of a stride cycle (more, if one accounts for the *double stance phases*, where both legs are in contact with the ground). Additionally, the feet periodically hit the ground at *heelstrike*, which marks the largest load acting on the biped during passive walking, and which also finds the knees at their fully extended state, and in the case of the 4B knees, around their singular configuration. Since these are both important features of passive walking, we will next explore the kinematics of the 4B knees around the singular configuration of Fig. 3(a).

In the following, we assume that the ground forces are the input to the 4B knees, and therefore we describe the motion of the kneecap angle θ_k as a function of the tibia angle θ_t. Using (9), we calculate pairs of angles (θ_t, θ_k) and use these to numerically estimate the partial derivative $\partial\theta_k/\partial\theta_t$, which is plotted in Fig. 4 for the 4B knees of Table I. In the same chart, we also plot the magnitude of corresponding partial derivative for the JK model. This is calculated from (2) and, as expected, it is found equal to 1 for every θ_k.

As can be seen in Fig. 4 the overall rate of change of the kneecap angle with respect to the tibial rotation in the 4B knees is significantly smaller than the corresponding rate of change in the JK knees.

In Fig. 4 the femoral links are assumed to be kept still at $\theta_f = 0$. The chart implies that for the same tibial rotation θ_t, the JK knees would exhibit a larger θ_k rotation than the 4B knees. Therefore, the kneecap moment of the JK biped would be larger for the same tibial rotation θ_t, effectively acting as a stiffer overall kneecap spring.

This is evidenced when we calculate the overall effective

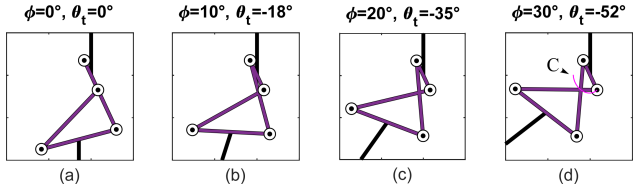

Fig. 3. (a) Singular configuration of 4B knee, for $\phi = 0$. (b-d) Configurations of 4B knee for constant $\theta_f = 0$ and various values of ${}^{4B}\theta_k = \phi$. The ICR, positioned at the intersection of the two crossing links, moves when the knee rotates, see curve C in (d).

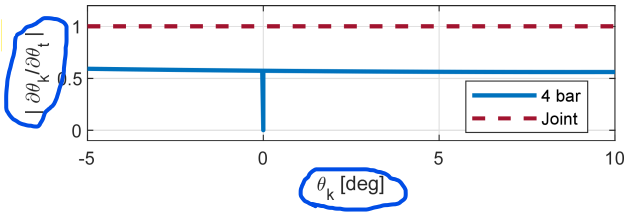

Fig. 4. Rate of change of the kneecap angle θ_k with respect to the rate of change of the tibial angle θ_t, for 4B and JK knees. The kneecap angle of the 4B knees will experience a smaller rotation than the corresponding angle on the JK knees, for the same tibial rotation θ_t. The singularity at the extended configuration of the 4B knees is evident at $\theta_k = 0$.

stiffness of the knees k_f, considering θ_t as the deformation input and T as the output torque acting on a fixed femur:

$$k_f = \frac{\partial T}{\partial \theta_t} = \frac{\partial T}{\partial \theta_k} \frac{\partial \theta_k}{\partial \theta_t} \tag{10}$$

Because the kneecaps used in the two models are mechanically the same, the term $\partial T/\partial \theta_k$ will be the same for the two models. However, according to Fig. 4 the term $\partial \theta_k/\partial \theta_t$ will be significantly larger in the JK model compared to the 4B model. Consequently, it will hold that:

$$^{\mathrm{JK}}k_f > ^{\mathrm{4B}}k_f \tag{11}$$

More importantly, at the singular configuration of the 4B knees, the effective stiffness of the 4B model will be instantaneously equal to zero, due to the singularity at that point, as observed in Fig. 4. This increased compliance of the 4B biped around the singular configuration will be in effect as the heel impacts the ground, and it is expected to significantly improve the impact behavior of the passive biped, as well as its ability to perform stable passive walking [5]. As the effective stiffness of the 4B knees is discontinuous, it is only equal to zero at the singular configuration and immediately jumps to a non-zero value for $^{\mathrm{4B}}\theta_k \neq 0$. Therefore, the increased singularity compliance is not expected to negatively affect the biped's overall ability to perform stable passive gait.

D. Analytical dynamic model

The dynamics of the JK biped have been described in detail in [8]. In the case of the 4B biped, the methodology followed to derive the dynamics is exactly the same. Therefore, the 4B biped's dynamic model is described briefly in this section, but the modeling details are spared in this paper to avoid repetition. The reader is urged to refer to [7] and [8] to find an in-depth description of the dynamics derivation.

The equations of motion of the 4B system are a Differential Algebraic Equation (DAE) system of the general form:

$$\begin{gathered} \mathbf{M(q)\ddot{q} + C(q,\dot{q})\dot{q} + K(q) + G(q) - f = 0} \\ \mathbf{Ws(q) = 0} \end{gathered} \tag{12}$$

In (12) $\mathbf{q}$ is the GC vector from (1) $\mathbf{M_{6x6}}$ is the inertia matrix of the 4B biped, $\mathbf{C_{6x1}}$ is the vector containing Coriolis, centrifugal and damping terms, and $\mathbf{K_{6x1}}$ and $\mathbf{G_{6x1}}$ are the stiffness and gravity force vectors respectively. The matrix $\mathbf{W_{4x4}}$:

$$\mathbf{W} = \mathrm{diag}(w_1, w_1, w_2, w_2) \tag{13}$$

is square diagonal, and acts as a *switching matrix*, in which $w_i = 0$ when leg-i is in swing and $w_i = 1$ when it is in stance. Therefore $\mathbf{W}$ activates the kinematic constraints $\mathbf{s_{4x1} = 0}$ in (12), which constrain a leg in stance to perform a rolling-without-slipping motion on the ground. There are two constraints for each leg: one for the rolling and one for the no-slipping constraint, and therefore there are a total of four constraints in $\mathbf{s}$. Finally, $\mathbf{f}$ is the constraint force vector, which is also switched on and off by $\mathbf{W}$:

$$\mathbf{f} = \left(\frac{\partial(\mathbf{Ws})}{\partial \mathbf{q}}\right)^{\mathrm{T}} \boldsymbol{\lambda} \tag{14}$$

where $\boldsymbol{\lambda_{4x1}}$ is the vector of Lagrange multipliers, containing the ground reaction forces that result from the constraints $\mathbf{s}$.

III. Simulations for two models of the knee

A. A close-up of the two bipeds' gaits

The dynamics of the two biped models are simulated in MATLAB using the DAE solver ode15s, which can handle DAEs and is effective and accurate for stiff systems. The JK and 4B models are identical except for their knee design, and therefore their dynamic behaviour is expected to be significantly similar.

Indeed, Fig. 5 shows the state space of the femoral and tibial angles, θ_f and θ_t respectively, for the JK and 4B bipeds, which are simulated for their response to identical Initial Conditions (ICs). The graphs present the state spaces for twenty consecutive steps of the bipeds. The selected ICs are outside of the stable passive trajectory of either model, but both models are able to converge to their respective passive trajectories after a few steps: this is evident from the plots of Fig. 5 (a) and (b), where the dashed lines appear solid from the superposition of many consecutive steps' data.

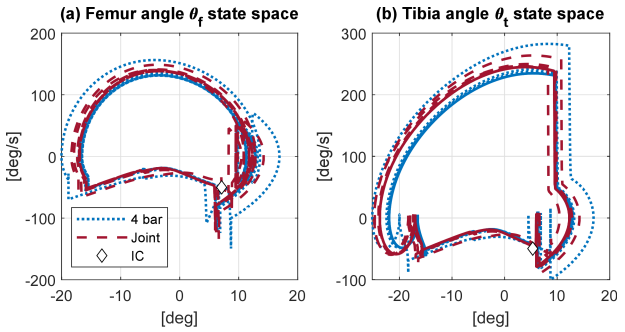

Fig. 5. State space of (a) femoral and (b) tibial leg angles, from simulations of 20 steps, for the JK and 4B biped models. The plots are read in a clockwise direction.

The stable passive trajectories of the JK and 4B bipeds in Fig. 5 appear to be almost identical for the femoral angle θ_f, while the tibial angle θ_t presents an increased tibial rotation during the swing phase.

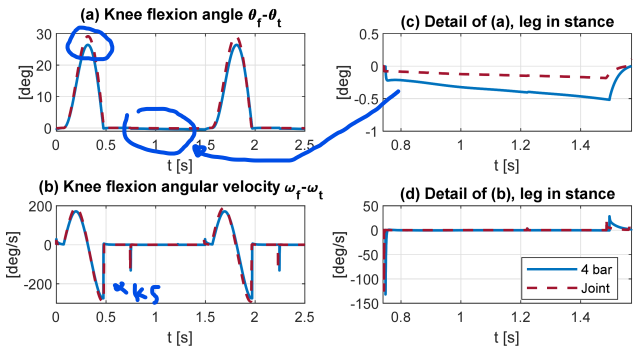

Fig. 6. (a) Knee flexion angles and (b) their velocities for four consecutive steps of the JK and 4B bipeds. (c-d) Stance phase details of (a) and (b).

This is evidenced more clearly in Fig. 6, where the overall knee flexion angles $\theta_f - \theta_t$ and the corresponding angular velocities $\omega_f - \omega_t$ of one leg of each biped are plotted for four consecutive steps of the JK and 4B bipeds. The four steps shown here are extracted from the 20-step simulations of Fig. 5, following the transient response and after the bipeds have both reached their steady state trajectories.

In these graphs one can easily identify two swing phases of the depicted legs between $t = [0.00, 0.75]s$ and $t = [1.50, 2.25]s$ from the large fluctuations of both Fig. 6 (a) and (b). Two knee strike occurrences are also identified at around $t = 0.5s$ and at $t = 2.00s$, which mark the activation of the kneecaps and are characterized by the sudden jumps in the angular velocity graphs of Fig. 6 (b). Finally, the legs' stance phases are those between a knee strike and the beginning of the next swing phase, for $t = [0.75, 1.50]s$ and after $t = 2.25s$. The stance phase for $t = [0.75, 1.50]s$ is also depicted in a closed-up view in Fig. 6 (c) and (d). It is worth noting that even though the model used in the simulations allows for a full dynamic simulation of the double stance phase (where two legs are in contact with the ground), this does not occur in these specific simulations, due to the increased stiffness of the models.

The larger swing-phase knee flexion of the JK biped compared to the 4B biped is attributed to the increased overall knee stiffness ${}^{\text{JK}}k_f$ from (11). Indeed, once the weight of the biped is transferred from a stance leg to the next, the former stance leg enters a swing phase, where the previously loaded knee will retract backwards in flexion.

Note that during a swing phase, the viscoelastic kneecaps are not activated and therefore the peaks of (11) are reached as the knees rotate freely. On the other hand, the depicted leg's knee flexion angles and their velocities during a stance phase, where the kneecaps support the weight of the bipeds, shown in detail in Fig. 6 (c) and (d), retain very small negative values, as the kneecaps prevent an increase in knee hyperextension. Fig. 6(c) showcases the increased stiffness of the JK biped, the knee extension of which is significantly more restricted during the stance phase.

Overall, the stable passive trajectories of the two models present similar dynamic responses with respect to their state variables. Next, the main descriptors of the bipeds' stable passive gaits will be compared.

B. Comparisons of key gait descriptors

Following the close-up comparison of the state variables of the two biped models, the JK and 4B bipeds are studied for their stable passive gait: this is the stable trajectory reached by the bipeds after their transient response to the ICs of Fig. 5, and once they have converged to their respective solid-line steady-state trajectories.

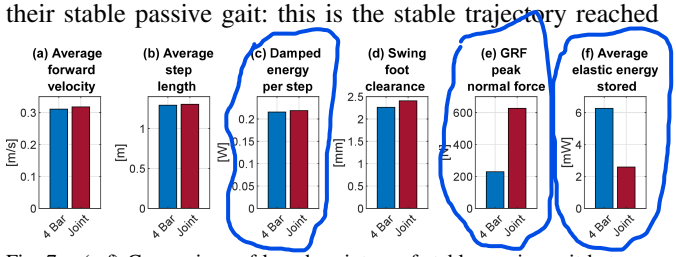

Fig. 7. (a-f) Comparison of key descriptors of stable passive gait between the JK and 4B bipeds.

Fig. 7 presents a few major gait descriptors of the stable passive gait of the JK and 4B bipeds. From the bar graphs (a) (b) and (c) it is evident that the average forward velocity, the average step length and the damped energy per step respectively are almost identical in the two bipeds.

The average forward velocity in (a) and the average step length (b) of the two bipeds are mainly governed by the pendulum dynamics of the bipeds' legs [5], and therefore heavily depend on the leg inertial distributions, which are almost identical for the two models.

On the other hand, the damped energy per step is a measure directly linked to the energetic loss of the bipeds, which, in a stable repetitive gait, has to be equal to the energetic gain from the descent within the gravitational field. As the two bipeds walk on the same slope in the simulations studied in this section, the energy damped per distance travelled is also expected to be the same [6]. The small difference observed in the damped energy per step (c) is due to the small difference in the average step length (b).

The swing foot clearance in (d) is the measure of the swing foot's minimum distance from the ground during its forward advancement at a swing phase. The kinetics of the 4B knees cause the swing foot of the 4B biped to follow a trajectory that is closer to the ground during its swing phase. This might be a drawback of the 4B design, as a smaller swing foot clearance might deem the biped susceptible to stub its toe, if there is a small obstacle on the ground.

Finally, the bar charts of (e) and (f) present dramatic differences between the two models.

First, the Ground Reaction Force (GRF) peaks (e) of the 4B biped are 64% less than those experienced by the JK biped. This is a direct result of the increased compliance of the 4B knees in (11), in both their general configuration and specifically in the singular one, which they hold at heel strike, when the GRFs obtain their peak values. The large decrease in the GRF peak values when using 4B knees can have significant effects on the durability of constructed biped robots, and it can improve the comfort of foot prostheses.

At last, the average elastic energy stored in (f) is more than twice in the 4B model compared to the JK model. This is expected, as the overall effective knee stiffness of the 4B model is smaller than the same parameter in the JK model, as was shown in (11). A more compliant system is expected to store larger amounts of energy in its elastic elements, which has been shown to aid passive stability in biped walkers [5].

IV. Results on Energetic Efficiency

As mentioned above, the increased overall compliance of the 4B kneed biped system, evidenced by the significantly larger amounts of elastic energy stored during its gait, hints at the possibility of the biped exhibiting increased parametric robustness with respect to gait stability [5]. Parametric robustness means that the model can withstand larger variations in its parameters, before losing its ability to perform stable

passive gaits. In this section, this claim is investigated, specifically regarding the parameter of the slope angle, α.

Bipeds that are able to perform stable passive gait on a smaller slopes have a smaller Cost of Transport (COT):

$$\text{COT} = \frac{\text{energy spent}}{\text{(biped's weight)(distance travelled)}} \tag{15}$$

A smaller COT translates to higher energetic efficiency. Specifically, if a stable passive gait exists for a biped on a slope α, then the gait's COT has been shown to be exactly $\text{COT} = \sin(\alpha)$ [6].

To investigate the hypothesis of increased parametric robustness, the initial slope angle of $\alpha = -1°$, on which both bipeds were previously shown to converge to stable passive trajectories, is gradually decreased in magnitude, approaching the theoretical limit value of $\alpha = 0$.

For each slope value α, the JK and 4B bipeds are given ICs from the known stable passive trajectory of the previously studied $\alpha - \Delta\alpha$. By keeping the steps $\Delta\alpha$ adequately small, the ICs given to the bipeds fall within the basins of attraction of the stable passive trajectory for the new slope angle, if such a trajectory exists. The bipeds are then simulated for 100 consecutive steps, which if successfully performed, indicate that a stable passive gait has been reached.

Fig. 8 shows this process for the JK and 4B biped models. It is observed that the JK biped loses its ability to perform stable passive gait at $\alpha = -0.52°$where COT$= 0.009$, while the 4B biped manages to exhibit stable passive gait until $\alpha = -0.39°$, corresponding to a minimum achieved COT of less than 0.007. This difference in minimum COT corresponds to 22% increase in gait efficiency when using the 4B knees instead of the JK knees.

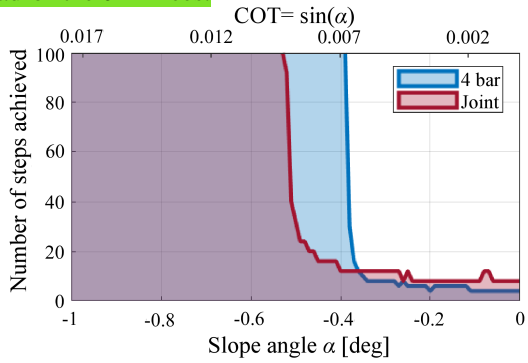

Fig. 8. Number of steps achieved by the JK and 4B biped models as the slope converges to $\alpha = 0$ and corresponding COT.

V. Conclusion

The results of this study showcase two significant advantages of using biomimetic four-bar linkages as knees in biped robots. First, it was found that the overall system stiffness of the four-bar kneed robot is significantly lower than that of the joint knee robot. The singular configuration of the biomimetic four-bar knees at heelstrike corresponds to locally zero stiffness values, contributing to this reduction. This increase in compliance reduces the maximum impact forces at heelstrike by 64% for the four-bar kneed robot. Additionally, the reduced system stiffness favors the energetic performance of the four-bar biped, which exhibits a COT reduction of 22%. We believe these results are significant in the study of gait dynamics, in the design of autonomous walking robots, and in the minimization of fatigue and discomfort of trans-femoral prostheses.

References

[1] T. McGeer, "Passive walking with knees," *Proc. IEEE International Conference on Robotics and Automation*, 1990, pp. 1640-1645.

[2] M. Garcia, et al., "The Simplest Walking Model: Stability, Complexity, and Scaling," in *J. of Biom. Eng.*, v. 120, no.2, pp. 281-288, Apr. 1998.

[3] F. Abi-Farraj, B. Henze, C. Ott, P. R. Giordano and M. A. Roa, "Torque-Based Balancing for a Humanoid Robot Performing High-Force Interaction Tasks," in *IEEE Robotics and Automation Letters*, vol. 4, no. 2, pp. 2023-2030, Apr. 2019.

[4] R. Alexander, "A model of bipedal locomotion on compliant legs," in *Phil. Trans. of the Royal Society of London, Series B: Biological Sciences*, vol. 338, no. 1284, pp. 189-198, Oct. 1992.

[5] A. Smyrli, G. Bertos, and E. Papadopoulos, 2021, "A generalized model for compliant passive bipedal walking: sensitivity analysis and implications on bionic leg design," *ASME Journal of Biomechanical Engineering* 143(10): 101008.

[6] A. Smyrli, M. Ghiassi, A. Kecskeméthy and E. Papadopoulos, "On the effect of semielliptical foot shape on the energetic efficiency of passive bipedal gait," *Proc. IEEE/RSJ International Conference on Intelligent Robots and Systems*, 2019, pp. 6302-6307.

[7] A. Smyrli and E. Papadopoulos, "A methodology for the incorporation of arbitrarily-shaped feet in passive bipedal walking dynamics," *Proc. IEEE Int. Conf. on Robotics and Automation*, 2020, pp. 8719-8725.

[8] A. Smyrli and E. Papadopoulos, "Modeling, Validation, and Design Investigation of a Passive Biped Walker with Knees and Biomimetic Feet," accepted in *Proc. IEEE International Conference on Robotics and Automation*, Philadelphia, PA, 2022.

[9] D. Owaki, et al., "A two-dimensional passive dynamic running biped with knees," *Proc. IEEE International Conference on Robotics and Automation*, 2010, pp. 5237-5242.

[10] Y. Ikemata, et al., "A study of the leg-swing motion of passive walking," *Proc. IEEE International Conference on Robotics and Automation*, 2008, pp. 1588-1593.

[11] G. Gini, U. Scarfogliero and M. Folgheraiter, "Human-Oriented Biped Robot Design: Insights into the Development of a truly Anthropomorphic Leg," *Proc. IEEE International Conference on Robotics and Automation*, 2007, pp. 2910-2915.

[12] Y. Liu, et al., "A bio-inspired knee joint for biped robots," *Proc. IEEE Int. Conf. on Information and Automation*, 2016, pp. 1387-1391.

[13] A. Hamon and Y. Aoustin, "Study of different structures of the knee joint for a planar bipedal robot," *Proc. IEEE-RAS International Conference on Humanoid Robots*, 2009, pp. 113-120.

[14] G. van Oort, et al., "An energy efficient knee locking mechanism for a dynamically walking robot," *Proc. IEEE International Conference on Robotics and Automation*, 2011, pp. 2003-2008.

[15] Y. Asano et al., "Biomimetic design of musculoskeletal humanoid knee joint with patella and screw-home mechanism," *Proc. IEEE Int. Conf. on Robotics and Biomimetics*, 2011, pp. 1813-1818.

[16] A. Hamon and Y. Aoustin, "Cross four-bar linkage for the knees of a planar bipedal robot," *Proc. IEEE-RAS International Conference on Humanoid Robots*, 2010, pp. 379-384.

[17] A. C. Etoundi, R. Vaidyanathan and S. C. Burgess, "A bio-inspired condylar hinge joint for mobile robots," *Proc. IEEE/RSJ International Conference on Intelligent Robots and Systems*, 2011, pp. 4042-4047.

[18] J. J. O'Connor, et al., "The geometry of the knee in the sagittal plane," in *Proc. of the Institution of Mechanical Engineers, Part H: Journal of Engineering in Medicine*, vol. 203, no.4, pp. 223-233, Dec. 1989.

[19] J. Bradley, et al., "Orientation of the cruciate ligament in the sagittal plane. A method of predicting its length-change with flexion," in *The Journal of Bone and Joint Surgery,* v. 70, no. 1, pp. 94-99, Jan. 1988.

[20] M. P. Greene, "Four bar linkage knee analysis," in *Orthotics and Prosthetics*, vol. 37, no. 1, pp. 15-24, 1983.

[21] C. W. Radcliffe, "Four-bar linkage prosthetic knee mechanisms: Kinematics, alignment and prescription criteria," in *Prosthetics and Orthotics International*, vol. 18, no. 3, pp. 159-173, Dec. 1994.

[22] J. De Vries, "Conventional 4-bar linkage knee mechanisms: a strength-weakness analysis," in *Journal of rehabilitation research and development,* vol. 32, no. 1, pp.36, Feb. 1995.